Check for updates

The simultaneous removal of cadmium (II) and lead (II) from wastewater with the application of green synthesized magnesium silicate hydrate

Zhang Qing[1,2]*, Liu Guijian[2,3], Peng Shuchuan[1]* and Zhou Chuncai[1,2]

[1]School of Resource and Environmental Engineering, Hefei University of Technology, Hefei, Anhui, China, [2]State Key Laboratory of Loess and Quaternary Geology, Institute of Earth Environment, The Chinese Academy of Sciences, Xi'an, Shaanxi, China, [3]CAS Key Laboratory of Crust-Mantle Materials and Environment, School of Earth and Space Sciences, University of Science and Technology of China, Hefei, Anhui, China

To the purpose of solving the problems of coal-gangue accumulation in the mine and pollution of cadmium (II) and lead (II) in wastewater, magnesium silicate hydrate (M-S-H) was synthesized from coal-gangue by thermochemical. M-S-H had removed Cd(II) and Pb(II) by adsorption. The characterization of M-S-H and adsorption effects factors, including initial solution pH, initial metal concentration, adsorbent dose, temperature, reaction time, and coexisting ions were explored for adsorption performance. The solution pH was precisely controlled by a pH meter. The adsorption temperature was controlled by a thermostatic gas bath oscillator with an error of ± 0.3. These results from this study revealed that M-S-H surface area increased from 8.12 to 26.15 m^2/g with a pore volume of 0.12 cm^3/g. The maximum adsorptions of Cd(II) and Pb(II) by M-S-H were 59.52 and 83.33 mg g^{-1}, respectively. The adsorption performance for Cd(II) and Pb(II) reached saturation at pH 5, temperature 25°C, M-S-H 6 g/L, reaction time 90 min, and metal concentration 300 mg/L. Cd(II) and Pb(II) adsorption were spontaneous and endothermic and well fitted with the pseudo-second-order kinetic and Langmuir isotherm adsorption models. The adsorption mechanisms were electrostatic interaction, ion exchange, and surface complexation. This research indicated that the synthesized M-S-H from coal gangue was efficiently eliminated metal ions from water, opening up new possibilities for coal gangue reuse.

Introduction

Due to the over-exploitation of mineral resources and rapid industrialization, the trace metal contamination of the water bodies had become a danger to human health and ecological stability (Li et al., 2019). Among the trace elements, cadmium (II) and lead (II) had been classified as the most toxic elements, and the release of these metals in the water had been strictly controlled (Gao et al., 2020). An excessive amount of Cd(II) and Pb(II) would influence human healthy *via* the food chain, causing severe abnormalities like lung cancer, neurasthenia, and Itai-Itai disease, impaired brain functions, and central nervous system (Zhang et al., 2010). Therefore, removing Cd(II) and Pb(II) from wastewater had become very important to provide clean water to the living bodies and gained significant importance for researchers (Zhang et al., 2021).

So far, multiple technologies were applied to eliminate Cd(II) and Pb(II) from wastewater, including complexation, chemical precipitation, adsorption, reverse osmosis, and electrodialysis (Liu and Zhang, 2018). Among these approaches, adsorption was considered the most acceptable treatment method because of its excellent efficiency, ease of handling, and economical (Jin et al., 2022; Sun et al., 2020). For this purpose, the choice of adsorbent was vital to achieving optimal performance. Commonly adsorbents for Cd(II) and Pb(II) removal contained biochar (Yu et al., 2021), cellulose (Qu et al., 2020), zero-valent iron nanoparticles (Febrianto et al., 2009), and activated carbon (Zhang et al., 2021). However, the majority of them were expensive and might result in secondary pollution. Thus, the development of cost-effective adsorbents exhibiting high adsorption capability, environment-friendly and long-term stability, green and straightforward operation, and effective regeneration focused on modern research.

Magnesium silicate hydrate (named M-S-H) was an excellent absorbent for eliminating toxic metal ions from wastewater (Liu et al., 2015; Nied et al., 2016). The primary chemical composition of M-S-H was $MgO-SiO_2-H_2O$, which could be varied within a specific range. The basic crystal structural unit of M-S-H was comparable to the 2:1 or 1:1 Mg-Si phyllosilicates (Lothenbach et al., 2015). Similarly, it previously reported that vermiculites had a crystal structural unit of M-S-H that could be efficient adsorption Cd and Pb in an aqueous solution (Alexandre-Franco et al., 2011). Moreover, sepiolite ($8MgO·12SiO_2·6H_2O·nH_2O$) could reduce available Pb from water and soil than microparticles (Alvani et al., 2019). The most popular approach for making M-S-H was to use magnesium oxide and silica fume at a high cost

and had considerable mass production limitations (Wang and Fan, 2020).

Currently, the synthesis of M-S-H from solid wastes or mineral matter as a raw material received further attention (Millán-Corrales et al., 2020). In this regard, China had a significant reserve of coal-gangue resources, which were of significant social and economic value. Coal-gangue was the most common industrial solid wastes, reaching approximately 4.5 billion tons in 2019 in China (Koshy et al., 2019). SiO_2 and Al_2O_3 were the main chemical constituents of coal-gangue. Previous studies had shown that modified coal-gangue had much potential for removing Cd and Pb from wastewater (Cao et al., 2016; Shang et al., 2019). However, the synthesized M-S-H from coal-gangue and its application in the water to remove metal ions were not studied.

Hence, the current research was planned to discuss the adsorptive interactions of Cd(II) and Pb(II) by M-S-H synthesized from coal-gangue with an aim to establish the adsorption isotherm and kinetics model. Furthermore, batch experiments, including initial metal concentrations, initial pH, adsorbent dose, temperature, reaction time, and coexistence ions, were performed. Finally, the adsorption mechanism was discovered according to adsorption data and characterization findings. This research provided a new method for synthesized M-S-H and removing heavy metals.

Materials and methods

Raw materials

Coal-gangue (named CG) was brought from the Guqiao coal mine, a traditional coal production site, in Huainan, Anhui Province, China. CG was mainly composed of Al_2O_3 and SiO_2, accounted for 81.64% of the total weight percent (Table 1). Besides, the CG surface area was 8.12 m^3/g, and pore volume was 0.016 cm^3/g. All chemicals used were analytical grade in the experiment, including $Mg(OH)_2$, $Pb(NO_3)_2$, $NaNO_3$, KNO_3, $Fe(NO_3)_3·9H_2O$, $Ca(NO_3)_2$, $Cd(NO_3)_2·4H_2O$, HNO_3, and NaOH. Deionized water was used throughout the tests.

Preparation of M-S-H

The CG sample was crushed to less than 2 cm using a boulder cracker and then dried at 80°C before grinding into power.

TABLE 1 Chemical content of coal gangue (wt%).

Sample	Al$_2$O$_3$	SiO$_2$	Fe$_2$O$_3$	SO$_3$	K$_2$O	Na$_2$O	MgO	CaO	LOI
CG	35.81	45.83	4.10	0.76	1.56	0.27	1.16	1.12	9.39

Subsequently, the sample was thoroughly blended with $Mg(OH)_2$, and the M Mg/Si ratio was 0.6. Afterward, the composite samples were calcinated at 700°C for 1 h in a Muffle furnace. Finally, the composite samples were cooled down and cured for 7 days at room temperature. The grain size of the synthesized M-S-H was 0.16 mm. The powdered phase was the original phase of the produced M-S-H.

Characterization methods

The specific surface area and pore diameter were explored with a specific surface area analyzer (Tristar II 3020 M, United States). X-ray fluorescence spectrometry (XRF-1800, Japan) was analyzed to characterize the primary composition of CG (wt%). Fourier transform infrared spectroscopy (FTIR, Nicolet 8,700, United States) was performed for the study of the structure; scanning electron microscopy (SEM, United States) was used for mineralogical composition, and X-ray powder diffraction (XRD, TTR-III, Japan) was explored to the microscopic morphology. Moreover, XRD patterns were recorded in the 2θ range (10–70°) with Cu-K (λ = 0.154 nm). The FTIR analysis of the samples was performed in the wavenumber between 400 and 4,000 cm^{-1}. The thermogravimetric analysis (TG) was performed on a Shimadzu DTG-60H instrument (Japan), heating between ambient temperature and 1,000°C in an N_2 atmosphere. The zeta potential was determined by a Zetasizer ZS instrument (NANOPLUS 3, United States). And surface elemental composition was measured by X-ray photoelectron spectrum (XPS, KRATOS, AXIS SUPRA+, United States).

Adsorption analysis

A series of 15 ml polyethylene tube containing 10 ml Cd(II) and Pb(II) solution with an initial metal concentration (25–1,000 mg/L) and initial pH (2.0–6.0) were added with a specific dose of M-S-H (2–10 g/L), then shaken at 200 rpm/min with various temperatures (25–45°C) and time (1–180 min) in a thermostatic gas bath oscillator, respectively. 0.1 M NaOH and HNO_3 adjusted the solution pH. The test error was controlled within ±0.3.

After adsorption, the liquids were separated from the solids after oscillation, followed by filtration with a 0.45 μm membrane. The filtrate samples were analyzed using an atomic absorption spectrometer (AAS, AA800, United States). The adsorption kinetics, isotherm, and thermodynamics models used during the adsorption analysis were performed in Supplementary Table S1 (Yousef et al., 2011).

Recycling performance of M-S-H was carried out as follows: 0.1 g of M-S-H was treated with 0.1 M HNO_3 solution for Cd(II) and Pb(II) desorption. The residue was rinsed with ethanol and water after the first oscillation, and the regenerated composite was tested for the repeated adsorption of Cd(II) and Pb(II) under the same condition.

Adsorption analysis in coexistence cation was performed as follows: 6 g/L M-S-H was mixed with Na^+, K^+, Ca^{2+}, and Fe^{3+}, respectively. The mixture oscillated for 90 min at 25°C and pH 5. The initial concentration was 300 mg/L for each cation. The pH value was kept constant during the experiment.

The adsorption capacity (qt, mg/g) was calculated by Eq. 1. In addition, the removal efficiency (E, %) was determined by Eq. 2 (Qu et al., 2020):

$$q_t = (C_0 - C_t)/m \qquad (1)$$

$$E = ((C_0 - C_t)/C_0) \times 100 \qquad (2)$$

where Co and Ct ($mg \cdot L^{-1}$) are the initial and final concentrations of metal in the solution, respectively, m (g) is the mass of adsorbent in 1 L solutions.

Results and discussion

Characterization of the CG and M-S-H

SEM presented that the CG surface was rough with large particles and irregular distribution (Figure 1A). However, the M-S-H particles were densely packed, with a regular and uniform distribution (Figure 1B). The CG flocculent particles adhered to the surface and pores of M-S-H after CG modification. Beyond that, the M-S-H surface area increased to 26.15 m^3/g with a pore volume of 0.12 cm^3/g, which provided many reactive binding sites for Cd(II) and Pb(II) adsorption (Wang et al., 2021).

XRD patterns showed that the significant mineralogical phases of the CG included kaolinite (Al_2O_3 $2SiO_2$ $2H_2O$) and quartz (SiO_2). Comparing the XRD patterns of CG, the kaolinite peaks in the M-S-H were almost absent (Figure 1C). Previous studies showed that the OH^- groups in kaolinite were gradually removed at high temperatures, destroying the internal mineral structure, then, the coordination of Al changed from octahedral ($[AlO_6]^{3-}$) to tetrahedral ($[AlO_4]^{5-}$), indicating its conversion to metakaolin (Al_2O_3 $2SiO_2$) (White et al., 2010). The presence of MgO peaks in the samples suggested the incomplete hydration of MgO. The broad peaks associated with M-S-H were observed in the 2θ range 20–42° ($4MgO \cdot 6SiO_2$ $7H_2O$) in CG. Sonat and Unluer supported the results that the dissolved silica amount played a crucial role in forming the hydrate phases (Sonat and Unluer, 2019).

Figure 1D presented the FTIR spectra of the samples cured for 7 days. Raw CG revealed the stretching vibrations of the outer and inner OH- groups at 3,696.39 and 3,620.70 cm^{-1}, respectively. Compared to the outer OH- groups, the inner OH- groups exhibited higher strength, and they were located
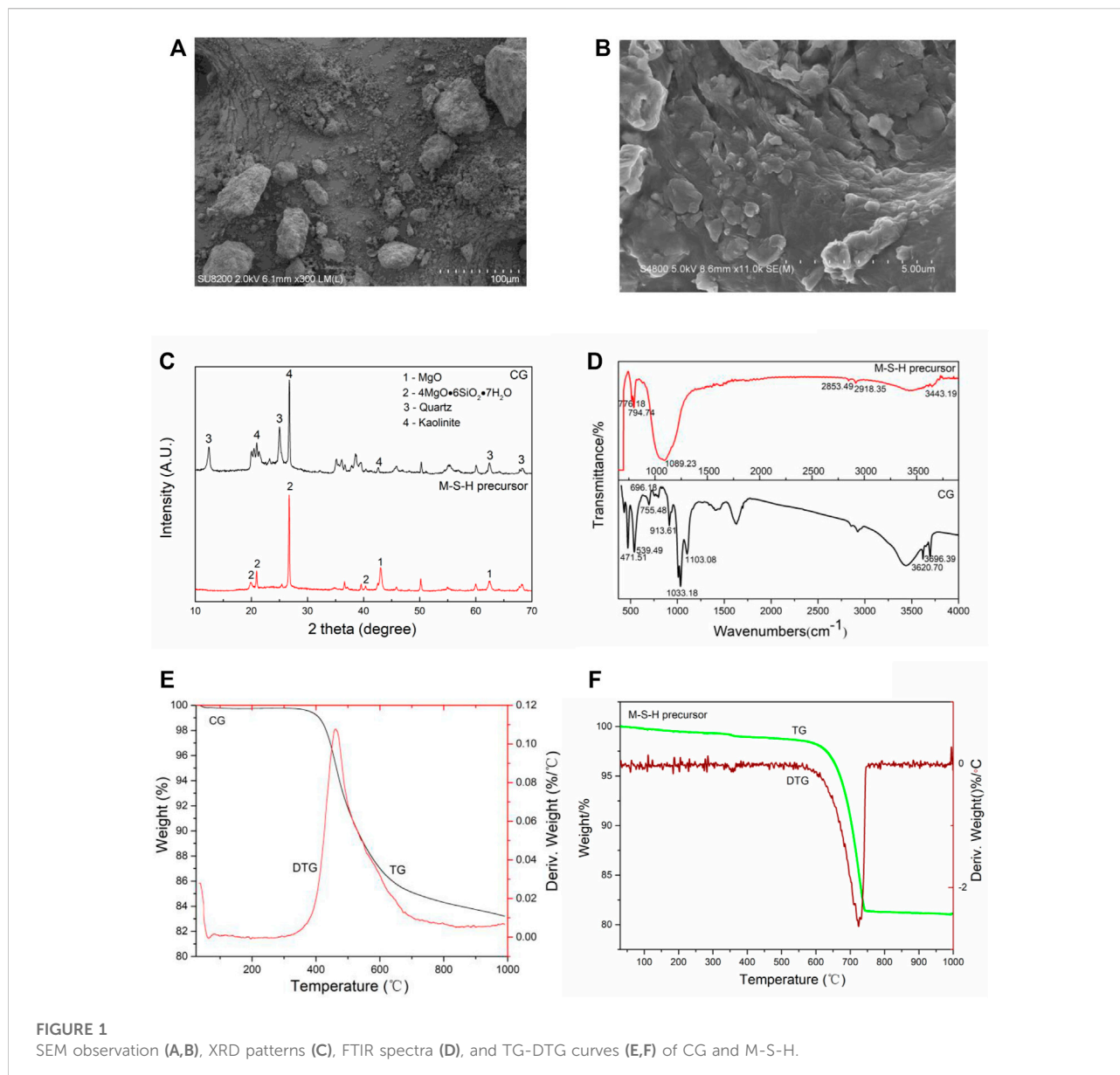
FIGURE 1
SEM observation **(A,B)**, XRD patterns **(C)**, FTIR spectra **(D)**, and TG-DTG curves **(E,F)** of CG and M-S-H.

between the tetrahedral and the octahedral sheets. The outer OH- groups could be combined with the oxygen atoms of the next tetrahedral layer to form weak hydrogen bonds (Fitos et al., 2015). The band at 913.61 cm^{-1} was corresponded to the Al-O-H vibration, while the Si-O-Alvi vibration was related to the band at 538.49 cm^{-1}. Similarly, the peaks at 1,103.08 and 755.48 cm^{-1} originated from the Si-O-Si groups. Moreover, the stretching peaks at 1,033.18, 696.18, and 471.51 cm^{-1} demonstrated the presence of Si-O-bands. For M-S-H, the bands at 3,443, 3,445, and 3,446 cm^{-1} were attributed to the stretching vibrations of the OH- groups in the crystal water. The early strength development in the samples might be associated with the formation of new hydroxyl bonds. The

bands at 2,918, 2,919, 2,921, 2,853, 2,854, and 2,856 cm^{-1} were attributed to the stretching vibrations of C-H. The bands at 1,089, 1,090, and 1,091 cm^{-1} represented the stretching vibrations of Si-O. The observed bands could have resulted due to the presence of the residual silica or the formation of new bands (i.e., Si-O-Mg bands). The bands at 776, 778, 794, 795 and 796 cm^{-1} originated from vibrations of the Si-O-Si bond.

The CG weight decreased marginally from ambient to 100°C because of the volatilization of adsorbed water and was in a clear downward trend from 300 to 750°C due to the fixed carbon combusting and volatiles escaping (Figure 1E). However, compared with CG, the initial mass loss of M-S-H was
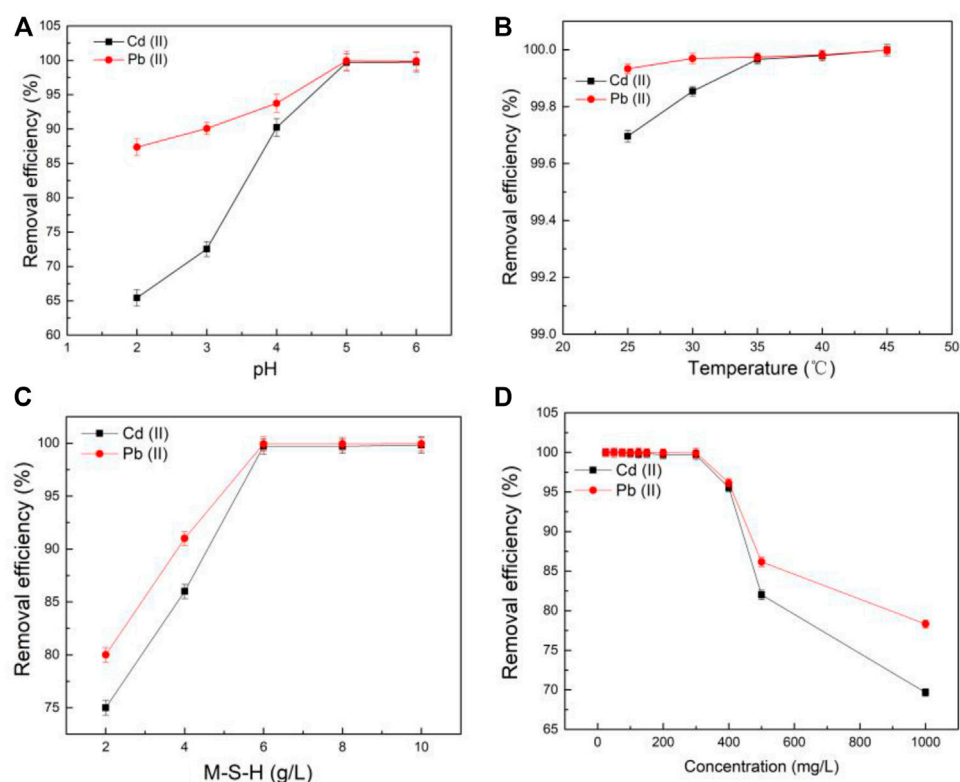
FIGURE 2
The effect of solution pH **(A)**, temperature **(B)**, M–S–H dosage **(C)**, and initial metals concentration **(D)** for adsorption (**(A)**, 25°C $[Cd(II)]_0$ = [Pb (II)]$_0$ = 300 mg/L, reaction time 90 min, 6 g/L M–S–H; **(B)**, pH 5 $[Cd(II)]_0$ = [Pb (II)]$_0$ = 300 mg/L, 90 min, 6 g/L M–S–H; **(C)**, 25°C, pH 5 $[Cd(II)]_0$ = [Pb (II)]$_0$ = 300 mg/L, 90 min; **(D)**, 25°C, pH 5, 90 min, 6 g/L M–S–H).

decreased slightly due to the evaporation of the interlayer and adsorbed water from ambient temperature to 600°C (Figure 1F). Subsequently, the mass loss increased significantly in the temperature range 600–780°C, and the OH^- groups had broken down (Lothenbach et al., 2015). After 780°C, the curves became smooth, and the weight loss of the M-S-H did not significantly change. These findings were suggesting that the thermal stability of the M-S-H was improved compared with CG.

Effect of solution pH

Solution pH had a significant effect on the chemical species and surface morphology of adsorbents (Xu et al., 2018). It could see that the pH of zero charge of the synthesized M-S-H was 3.2 (Figure 2A). Thus, the M-S-H was positively charged at a pH of 2–3.2 and negatively charged in a range of pH 3.2–6. At pH < 3.2, the positive charges on the M-S-H surface enhanced the repulsive forces between the metal cations and other protons for the binding sites, leading to a decrease in heavy metals removal performance (Jiang et al., 2018). Beyond that, the corresponding

functional groups in the M-S-H, such as Al-OH and Si-OH, were hard to protonate to form complexes with Cd(II) and Pb(II) (Bernard et al., 2019; Roosz et al., 2015).

The solution pH value after the adsorption was increased from 5.6 to 5.9. At pH > 3.2, the M-S-H with negatively charged had strong electrostatic interactions to adsorption

TABLE 2 Freundlich and Langmuir isotherms for Cd(II) and Pb(II) adsorption.

Adsorbate	Isothrom	Parameters		R^2
Cd	Freundlich	$K_F (L \cdot mg^{-1})$	N	0.85
		12.49	4.01	
	Langmuir	q_m (mg·g^{-1})	K_L (L·mg^{-1})	0.98
		59.52	0.05	
		534.32	45.69	
Pb	Freundlich	$K_F (L \cdot mg^{-1})$	N	0.80
		21.31	3.67	
	Langmuir	q_m (mg·g^{-1})	K_L (L·mg^{-1})	0.99
		83.33	0.43	

TABLE 3 Comparison of Cd(II) and Pb(II) adsorption onto M-S-H synthesized by coal-gangue with other adsorbents.

Adsorbent	Pollutant	q_{max} (mg/g)	References
Biomass-derived carbon	Cd(II)	40.65	Guo et al. (2017)
Nanoscale zero-valent iron		48.63	Li et al. (2018)
Modified fly ash		56.31	Huang et al. (2020)
coal fly ash		32.98	Wang et al. (2018)
Sepiolite	Pb (II)	34.7	Alvani et al. (2019)
Chitosan-pyromellitic dianhydride modified biochar		13.98	Deng et al. (2017)
Oxidized pine wood hydrochar		46.7	Madduri et al. (2020)
Hydrochar/Mg/Al-LDHs composites		62.4	Luo et al. (2020)
M-S-H	Cd(II)	59.52	This study
	Pb (II)	83.33	

TABLE 4 Thermodynamic parameters for Cd(II) and Pb(II) adsorption.

Adsorbate	Temperature (C)	K_0	ΔG^0 (kJ·mol^{-1})	ΔH^0 (kJ·mol^{-1})	ΔS^0 (J·mol^{-1}·K^{-1})
Cd	25	2,499.9	−20.27	62.04	146.02
	30	833.23	−20.48		
	35	624.90	−20.95		
	40	499.90	−23.38		
	45	416.57	−23.95		
Pb	25	2,499.9	−21.02	57.23	125.48
	30	2,272.63	−21.61		
	35	1785.61	−23.17		
	40	833.23	−23.47		
	45	624.90	−24.38		

Cd(II) and Pb(II) in the solution. Besides, the Al-OH and Si-OH groups deprotonated with the increased OH⁻ and provided more adsorption sites for the surface complexation reaction with Cd(II) and Pb(II), which was more supportive for adsorption (Xu et al., 2020). Moreover, Pb(II) had a larger diameter and electric negativity than Cd(II). So, the removal efficiency of Cd(II) was lower than that of Pb(II) at pH 2–6.

The result of this work revealed that the solution pH was related to the removal of Cd(II) and Pb(II) by synthesized M-S-H. Moreover, the removal efficiency was enhanced with the solution pH rose, reaching 99.00% at pH 6, suggesting that the solution pH significantly contributed to the metal adsorption. It also found some precipitates in the aqueous solution at pH 6. Hence, from the results, pH 5 was considered to be the optimal pH for further research.

Effect of temperature and M-S-H dosage and initial metals concentration

From Figure 2B, the adsorption efficiency of Cd(II) and Pb(II) was improved as the temperature increased, indicated an endothermic process (Shang et al., 2019). This was because that the breaking of bonds (e.g., Al-OH and Si-OH) required to absorb energy, while the binding of bonds with Cd(II) and Pb(II) needed to release energy. M-S-H could provide more binding sites for adsorption when the breaking rate of old bands was higher than the formation of new bands. The removal efficiency of Cd(II) and Pb(II) already reached over 99.00% at 25°C. So, the temperature at 25°C was selected for further study from the perspective of energy saving.

Besides, a larger dosage of the M-S-H could provide more reactive binding sites, function groups, porous structure, and surface area, leading to the removing Cd(II) and Pb(II) increased considerably. The Cd(II) and Pb(II) had been almost removed at
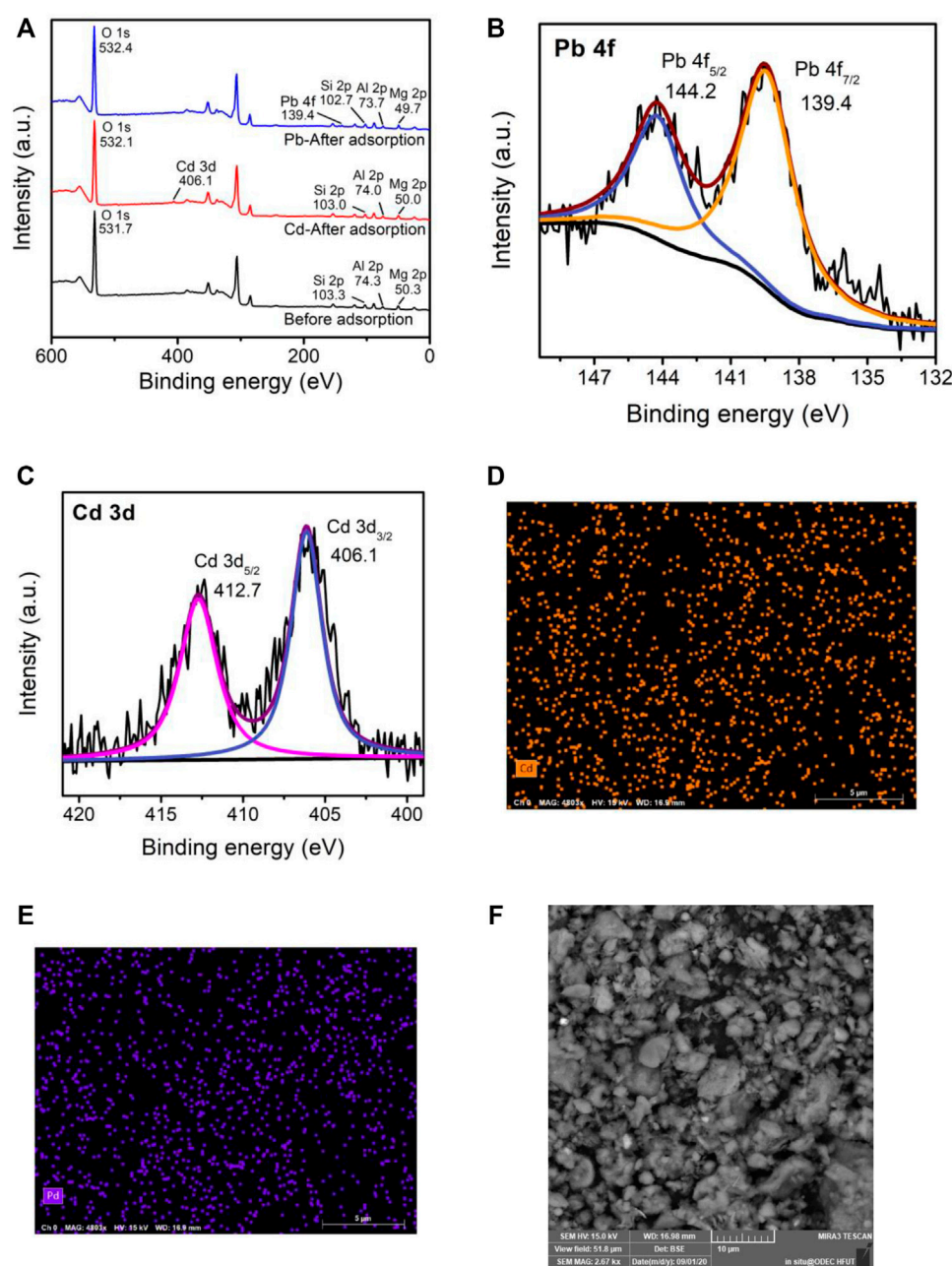
FIGURE 3
The XPS spectra **(A–C)** and SEM-ESD **(D–F)** of M-S-H before and after adsorption of Cd(II) and Pb(II).

M-S-H of 6.0 g/L within an initial metal concentration of 300 mg/L (Figure 2C,D).

Adsorption kinetics

The most effective adsorption mechanism and time could be obtained by fitting the kinetic adsorption parameters (Zhao et al., 2016). Moreover, the kinetic adsorption models for Cd(II) and

Pb(II) displayed similar trends (Supplementary Figure S1). The instantaneous adsorption of Cd(II) and Pb(II) enhanced sharply in the first 30 min due to the instant diffusion of metal ions to adsorption sites on the outer surface of the material in the aqueous solution. Then, the adsorption capacity gradually decreased, suggesting metal ions entered the internal pores of M-S-H during the 30–90 min. The adsorption capacity slowly rose to a stable value until the adsorption reached an equilibrium state from 90 to 180 min due to the enhanced diffusion resistance

in the pores. The two kinds of kinetic models were displayed in Eqs 3, 4 (Supplementary Table S1), respectively. The correlation coefficient (R12 > 0.99) of the pseudo-second-order kinetic model was observed to be much higher than that of the pseudo-first-order kinetic model (Supplementary Table S2). In other words, the pseudo-second-order kinetic model effectively fitted the adsorption process of Cd(II) and Pb(II).

Adsorption isotherms

Freundlich and Langmuir adsorption isotherms were applied to explore Cd(II) and Pb(II) sorption behavior on M-S-H. The non-linear forms of the adsorption isotherm models were expressed in Eqs 5, 6 (Supplementary Table S1). The Langmuir isotherm model described a uniformly and monolayer adsorption (Eq. 5), while the Freundlich isotherm model supposed that the sorption happened on the heterogeneous adsorbent surface in the form of multi-layers (Eq. 6). As observed from Supplementary Figure S1 and Table 2, the adsorption data of Cd(II) and Pb(II) exhibited a superior R^2 value, confirming the homogenous monolayer on the adsorbents. The Langmuir isotherm model showed that the maximum adsorptions of the M-S-H for Cd(II) and Pb(II) were 59.52 and 83.33 mg/g, respectively. Table 3 confirmed that M-S-H developed in this study exhibits superior adsorption performance than the previously reported adsorbents.

Adsorption thermodynamics

Enthalpy change (ΔH^0, kJ·mol^{-1}), Gibbs free energy (ΔG^0, kJ·mol^{-1}) and entropy change (ΔS^0, J·mol^{-1}·K^{-1}) were expressed as Eqs 7–10 (Supplementary Table S1), respectively. They determined the possibility of adsorption and the degree of difficulty of the

FIGURE 4
The adsorption mechanisms of Cd(II) and Pb(II) onto M-S-H.

adsorption process. In general, the ΔG^0 value for the physical adsorption ranged from −20.0 to 0.0 kJ mol^{-1}, and the physicochemical adsorption ranged from −80.0 to −20.0 kJ mol^{-1}, while the chemisorption was between −40.0 and −80 kJ mol^{-1} (Schwaab et al., 2017). From Table 4, the negative values of ΔG^0 presented that the process was spontaneous physicochemical adsorption on the liquid-solid interface. Furthermore, it was more favorable to adsorption at higher temperatures due to a lower ΔG^0 value with the increasing temperature from 25 to 45°C. The positive values of ΔH^0 and ΔS^0 once again proved the endothermic nature and increased entropy during adsorption. It confirmed that the randomness of the liquid-solid interface was enhanced as the adsorption proceeded (Xu et al., 2020).

## Recycling and regeneration performance

Recycling and regeneration performance were important indexes to evaluate the process efficiency and economic benefit of an adsorbent. The experimental data were carried out at $[Cd(II)]_0 = [Pb(II)]_0 = 300$ mg/L, 25°C, 90 min, pH 5 and M-S-H 6 g/L. Although the removal efficiency of Cd(II) and Pb(II) was dropped with the cycle number increased (Supplementary Figure S3), the removal efficiency remained relatively high (86.35% for Cd(II) and 84.21% for Pb(II)) despite six adsorption/desorption cycles. These results showed that the M-S-H had an excellent recyclability property for multi-time usage.

Effect of coexisting ions

It usually contained many coexisting ions in the contaminated wastewater, such as Na$^+$, K$^+$, Ca^{2+}, and Fe^{3+}. The coexisting ions Ca^{2+} and Fe^{3+} had a significant effect on removing Cd(II) and Pb(II) (Supplementary Figure S4). However, Cd(II) and Pb(II) removal changed little with Na$^+$ and K$^+$ presented in the solution, respectively. The high valent ions (Ca^{2+} and Fe^{3+}) had an advantage over lower valent ions (Na+ and K+), which could be preemptive combine with the functional groups on the M-S-H and unfavorable for Cd(II) and Pb(II) adsorption (Wen et al., 2017).

Adsorption mechanism

To further understand the sorption mechanism of Cd(II) and Pb(II) on M-S-H, the XPS spectra and SEM-EDS of M-S-H before and after adsorption of Cd(II) and Pb(II) were presented in Figure 3. According to the XPS spectra analysis, the prominent peaks of the M-S-H before adsorption ions were Mg 1s, Si 2p, Al 2p, and O1s (Figure 3A). The Cd 3 days and Pb 4f peaks were observed after M-S-H adsorption, suggesting that Cd(II) and Pb were successfully adsorption on M-S-H. Furthermore, the peak intensities of Mg 1s, Si 2p, and Al 2p decreased significantly after adsorption Pb(II) than that after adsorption Cd(II). The O1s peak of M-S-H was 531.7 eV
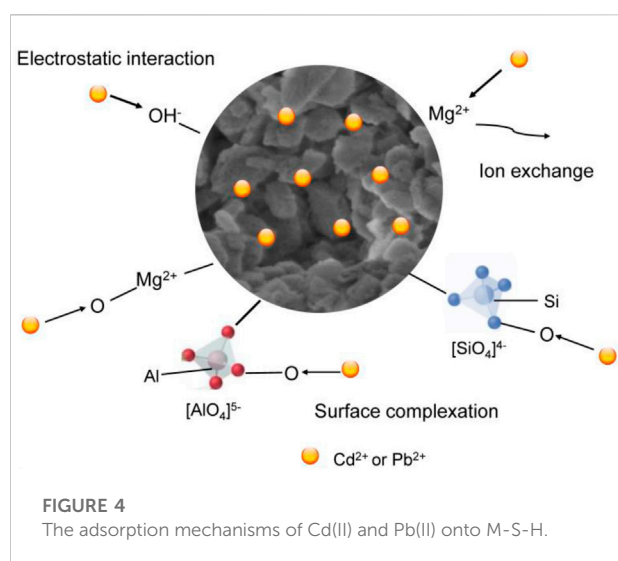
and increased 532.1 eV and 532.4 eV after adsorption, respectively. These results indicated that the functional groups had a greater affinity to form Pb-O than Cd-O, such as Mg-O, Si-OH, and Al-OH (Zhang et al., 2021). The Cd 3 days spectrum was divided into two peaks at 412.7 eV (Cd $3d_{5/2}$) and 406.1 eV (Cd $3d_{3/2}$), attributed to cadmium silicate and oxide (Figure 3B) (Sun et al., 2018). Similarly, peaks at 144.2 eV (Pb $4f_{5/2}$) and 139.4 eV (Pb $4f_{7/2}$) were corresponded to lead silicate and oxide (Figure 3C) (Nied et al., 2016). The SEM-EDS mapping showed that the Cd^{2+} sites overlapped with most Pb^{2+} (Figures 3D,E). After adsorption, the structure of M-S-H became more condensed, and the internal pore diameter became smaller after being filled with ions (Figure 3F).

To sum up, there were three possible adsorption mechanisms (Figure 4). First, at pH > 3.2, M-S-H with negatively charged had strong electrostatic interactions to adsorption Cd(II) and Pb(II). Second, Mg^{2+} was replaced with Cd^{2+} to form a crystalline or phase containing Cd silicate due to the similar electronegativity and the ionic radius of Cd^{2+} to Mg^{2+} (Gougar et al., 1996). Pb^{2+} was stabilized in the interlamellar structure and attached to the silica tetrahedron at the end of the M-S-H after replaced Mg^{2+}. Thus, Cd^{2+} and Pb^{2+} could replace Mg^{2+} by ion exchange in the M-S-H. Finally, surface complexation with Mg-O/Si-OH/Al-OH formed Cd(II) and Pb(II) complexes, such as Mg-O-Cd/Pb, Si-O-Cd/Pb, and Al-O-Cd/Pb.

Conclusion

In our work, the M-S-H was successfully synthesized from coal-gangue by thermochemical, providing a practical use for coal-gangue. For M-S-H, the surface area increased to 26.15 m^3/g with a pore volume of 0.12 cm^3/g. Moreover, the coordination of Al changed from octahedral to tetrahedral, and the kaolinite peaks were almost absent. The thermal stability of M-S-H was improved. M-S-H exhibited excellent adsorption properties for use as an adsorbent for removing water contaminants. The pseudo-second-order kinetic and Langmuir isotherm models effectively described the adsorption behavior of Cd(II) and Pb(II). The adsorption mechanisms were electrostatic interaction, ion exchange, and surface complexation. The adsorption performance for Cd(II) and Pb(II) reached saturation at pH 5, temperature 25°C, M-S-H 6 g/L, reaction time 90 min, and metal concentration 300 mg/L. The maximum adsorptions of Cd(II) and Pb(II) by M-S-H were 59.52 and 83.33 $mg\,g^{-1}$, respectively. The M-S-H may also be used to remove other cations in practical applications, such as silver and mercury, explored in the future.

Data availability statement

The original contributions presented in the study are included in the article/supplementary material, further inquiries can be directed to the corresponding author.

Author contributions

ZQ designed and conducted all the experiments, wrote, and revised the manuscript; LG supervised and revised the manuscript; PS provided assistance for data acquisition and analysis; ZC carried out the manuscript preparation and literature search. All authors have read and approved the content of the manuscript.

Funding

Acknowledgments

Conflict of interest

The authors declare that the research was conducted in the absence of any commercial or financial relationships that could be construed as a potential conflict of interest.

Publisher's note

All claims expressed in this article are solely those of the authors and do not necessarily represent those of their affiliated organizations, or those of the publisher, the editors and the reviewers. Any product that may be evaluated in this article, or claim that may be made by its manufacturer, is not guaranteed or endorsed by the publisher.

Supplementary material

The Supplementary Material for this article can be found online at: https://www.frontiersin.org/articles/10.3389/feart.2022.1074687/full#supplementary-material

References

Alexandre-Franco, M., Albarrán-Liso, A., and Gómez-Serrano, V. (2011). An identification study of vermiculites and micas. *Fuel Process. Technol.* 92, 200–205. doi:10.1016/j.fuproc.2010.03.005

Alvani, S., Hojati, S., and Landi, A. (2019). Effects of sepiolite nanoparticles on the kinetics of Pb and Cu removal from aqueous solutions and their immobilization in columns with different soil textures. *Geoderma* 350, 19–28. doi:10.1016/j.geoderma.2019.05.004

Bernard, E., Lothenbach, B., Pochard, I., and Cau-Dit-Coumes, C. (2019). Alkali binding by magnesium silicate hydrates. *J. Am. Ceram. Soc.* 102, 6322–6336. doi:10.1111/jace.16494

Cao, Z., Cao, Y., Dong, H., Zhang, J., and Sun, C. (2016). Effect of calcination condition on the microstructure and pozzolanic activity of calcined coal gangue. *Int. J. Mineral Process.* 146, 23–28. doi:10.1016/j.minpro.2015.11.008

Deng, J., Liu, Y., Liu, S., Zeng, G., Tan, X., Huang, B., et al. (2017). Competitive adsorption of Pb(II), Cd(II) and Cu(II) onto chitosan-pyromellitic dianhydride modified biochar. *J. Colloid Interface Sci.* 506, 355–364. doi:10.1016/j.jcis.2017.07.069

Febrianto, J., Kosasih, A. N., Sunarso, J., Ju, Y. H., Indraswati, N., and Ismadji, S. (2009). Equilibrium and kinetic studies in adsorption of heavy metals using biosorbent: A summary of recent studies. *J. Hazard. Mater.* 162, 616–645. doi:10.1016/j.jhazmat.2008.06.042

Fitos, M., Badogiannis, E. G., Tsivilis, S. G., and Perraki, M. (2015). Pozzolanic activity of thermally and mechanically treated kaolins of hydrothermal origin. *Appl. Clay Sci.* 116-117, 182–192. doi:10.1016/j.clay.2015.08.028

Gao, R., Hu, H., Fu, Q., Li, Z., Xing, Z., Ali, U., et al. (2020). Remediation of Pb, Cd, and Cu contaminated soil by co-pyrolysis biochar derived from rape straw and orthophosphate: Speciation transformation, risk evaluation and mechanism inquiry. *Sci. Total Environ.* 730, 139119. doi:10.1016/j.scitotenv.2020.139119

Gougar, M. L. D., Scheetz, B. E., and Roy, D. (1996). Ettringite and C-S-H Portland cement phases for waste ion immobilization: A review. *Waste Manag.* 16, 295–303. doi:10.1016/s0956-053x(96)00072-4

Guo, Z. Z., Zhang, X. D., Kang, Y., and Zhang, J. (2017). Biomass-Derived carbon sorbents for Cd(II) removal: Activation and adsorption mechanism. *ACS Sustain. Chem. Eng.* 5, 4103–4109. doi:10.1021/acssuschemeng.7b00061

Huang, X., Zhao, H., Zhang, G., Li, J., Yang, Y., and Ji, P. (2020). Potential of removing Cd(II) and Pb(II) from contaminated water using a newly modified fly ash. *Chemosphere* 242, 125148. doi:10.1016/j.chemosphere.2019.125148

Jiang, L. Y., Ye, Q. C., Chen, J. M., Zhong, C., and Gu, Y. L. (2018). Preparation of magnetically recoverable bentonite-Fe$_3$O$_4$-MnO$_2$ composite particles for Cd(II) removal from aqueous solutions. *J. Colloid Interface Sci.* 513, 748–759. doi:10.1016/j.jcis.2017.11.063

Jin, Y., Liu, Z., Han, L., Zhang, Y., Li, L., Zhu, S., et al. (2022). Synthesis of coal-analcime composite from coal gangue and its adsorption performance on heavy metal ions. *J. Hazard. Mater.* 423, 127027.

Koshy, N., Dondrob, K., Hu, L., Wen, Q., and Meegoda, J. N. (2019). Synthesis and characterization of geopolymers derived from coal gangue, fly ash and red mud. *Constr. Build. Mater.* 206, 287–296. doi:10.1016/j.conbuildmat.2019.02.076

Li, J., Zheng, L., Wang, S. L., Wu, Z., Wu, W., Niazi, N. K., et al. (2019). Sorption mechanisms of lead on silicon-rich biochar in aqueous solution: Spectroscopic investigation. *Sci. Total Environ.* 672, 572–582. doi:10.1016/j.scitotenv.2019.04.003

Li, Z., Wang, L., Meng, J., Liu, X., Xu, J., Wang, F., et al. (2018). Zeolite-supported nanoscale zero-valent iron: New findings on simultaneous adsorption of Cd(II), Pb(II), and As(III) in aqueoussolution and soil. *J. Hazard. Mater.* 344, 1–11. doi:10.1016/j.jhazmat.2017.09.036

Liu, L., and Zhang, K. (2018). Nanopore-based strategy for sequential separation of heavy-metal ions in water. *Environ. Sci. Technol.* 52, 5884–5891. doi:10.1021/acs.est.7b06706

Liu, M., Wang, Y., Chen, L., Zhang, Y., and Lin, Z. (2015). Mg(OH) 2 supported nanoscale zero valent iron enhancing the removal of Pb(II) from aqueous solution. *ACS Appl. Mater. Interfaces* 7, 7961–7969. doi:10.1021/am509184e

Lothenbach, B., Nied, D., L'Hôpital, E., Achiedo, G., and Dauzères, A. (2015). Magnesium and calcium silicate hydrates. *Cem. Concr. Res.* 77, 60–68. doi:10.1016/j.cemconres.2015.06.007

Luo, X., Huang, Z., Lin, J., Li, X., Qiu, J., Liu, J., et al. (2020). Hydrothermal carbonization of sewage sludge and *in-situ* preparation of hydrochar/MgAl-layered double hydroxides composites for adsorption of Pb(II). *J. Clean. Prod.* 258, 120991. doi:10.1016/j.jclepro.2020.120991

Madduri, S., Elsayed, I., and Hassan, E. B. (2020). Novel oxone treated hydrochar for the removal of Pb(II) and methylene blue (MB) dye from aqueous solutions. *Chemosphere* 260, 127683. doi:10.1016/j.chemosphere.2020.127683

Millán-Corrales, G., González-López, J. R., Palomo, A., and Fernandez-Jiménez, A. (2020). Replacing fly ash with limestone dust in hybrid cements. *Constr. Build. Mater.* 243, 118169. doi:10.1016/j.conbuildmat.2020.118169

Nied, D., Enemark-Rasmussen, K., L'Hopital, E., Skibsted, J., and Lothenbach, B. (2016). Properties of magnesium silicate hydrates (M-S-H). *Cem. Concr. Res.* 79, 323–332. doi:10.1016/j.cemconres.2015.10.003

Qu, J., Tian, X., Jiang, Z., Cao, B., Akindolie, M. S., Hu, Q., et al. (2020). Multi-component adsorption of Pb(II), Cd(II) and Ni(II) onto microwave-functionalized cellulose: Kinetics, isotherms, thermodynamics, mechanisms and application for electroplating wastewater purification. *J. Hazard. Mater.* 387, 121718. doi:10.1016/j.jhazmat.2019.121718

Roosz, C., Grangeon, S., Blanc, P., Montouillout, V., Lothenbach, B., Henocq, P., et al. (2015). Crystal structure of magnesium silicate hydrates (M-S-H): The relation with 2:1 Mg-Si phyllosilicates. *Cem. Concr. Res.* 73, 228–237. doi:10.1016/j.cemconres.2015.03.014

Schwaab, M., Steffani, E., Barbosa-Coutinho, E., and Severo Júnior, J. B. (2017). Critical analysis of adsorption/diffusion modelling as a function of time square root. *Chem. Eng. Sci.* 173, 179–186. doi:10.1016/j.ces.2017.07.037

Shang, Z., Zhang, L., Zhao, X., Liu, S., and Li, D. (2019). Removal of Pb(II), Cd(II) and Hg(II) from aqueous solution by mercapto-modified coal gangue. *J. Environ. Manag.* 231, 391–396. doi:10.1016/j.jenvman.2018.10.072

Sonat, C., and Unluer, C. (2019). Development of magnesium-silicate-hydrate (M-S-H) cement with rice husk ash. *J. Clean. Prod.* 211, 787–803. doi:10.1016/j.jclepro.2018.11.246

Sun, J., Chen, Y., Yu, H., Yan, L., Du, B., and Pei, Z. (2018). Removal of Cu(2+), Cd(2+) and Pb(2+) from aqueous solutions by magnetic alginate microsphere based on Fe$_3$O$_4$/MgAl-layered double hydroxide. *J. Colloid Interface Sci.* 532, 474–484. doi:10.1016/j.jcis.2018.07.132

Sun, Z., Liu, Y., and Hong, W. (2020). Facile synthesis of porous hydrated magnesium silicate adsorbent from ordinary silica gel. *Mater. Lett.* 272, 127886. doi:10.1016/j.matlet.2020.127886

Wang, B., and Fan, C. (2020). Hydration behavior and immobilization mechanism of MgO-SiO$_2$-H$_2$O cementitious system blended with MSWI fly ash. *Chemosphere* 250, 126269. doi:10.1016/j.chemosphere.2020.126269

Wang, B., Ma, Y., Lee, X., Wu, P., Liu, F., Zhang, X., et al. (2021). Environmental-friendly coal gangue-biochar composites reclaiming phosphate from water as a slow-release fertilizer. *Sci. Total Environ.* 758, 143664. doi:10.1016/j.scitotenv.2020.143664

Wang, B., Zhou, Y., Li, L., Xu, H., Sun, Y., and Wang, Y. (2018). Novel synthesis of cyano-functionalized mesoporous silica nanospheres (MSN) from coal fly ash for removal of toxic metals from wastewater. *J. Hazard. Mater.* 345, 76–86. doi:10.1016/j.jhazmat.2017.10.063

Wen, T., Wang, J., Yu, S., Chen, Z., Hayat, T., and Wang, X. (2017). Magnetic porous carbonaceous material produced from tea waste for efficient removal of as(V), Cr(VI), humic acid, and dyes. *ACS Sustain. Chem. Eng.* 5, 4371–4380. doi:10.1021/acssuschemeng.7b00418

White, C. E., Provis, J. L., Proffen, T., Riley, D. P., and Deventer, J. V. (2010). Density functional modeling of the local structure of kaolinite subjected to thermal dehydroxylation. *J. Phys. Chem. A* 114, 4988–4996. doi:10.1021/jp911108d

Xu, H., Hu, X., Chen, Y., Li, Y., Hu, X., Tang, C., et al. (2020). Cd(II) and Pb(II) absorbed on humic acid-iron-pillared bentonite: Kinetics, thermodynamics and mechanism of adsorption. *Colloids Surfaces A Physicochem. Eng. Aspects* 612, 126005. doi:10.1016/j.colsurfa.2020.126005

Xu, W., Song, Y., Dai, K., Sun, S., Liu, G., and Yao, J. (2018). Novel ternary nanohybrids of tetraethylenepentamine and graphene oxide decorated with MnFe2O4 magnetic nanoparticles for the adsorption of Pb(II). *J. Hazard. Mater.* 358, 337–345. doi:10.1016/j.jhazmat.2018.06.071

Yousef, R. I., El-Eswed, B., and Al-Muhtaseb, A. a. H. (2011). Adsorption characteristics of natural zeolites as solid adsorbents for phenol removal from aqueous solutions: Kinetics, mechanism, and thermodynamics studies. *Chem. Eng. J.* 171, 1143–1149. doi:10.1016/j.cej.2011.05.012

Yu, W., Hu, J., Yu, Y., Ma, D., Gong, W., Qiu, H., et al. (2021). Facile preparation of sulfonated biochar for highly efficient removal of toxic Pb(II) and Cd(II) from wastewater. *Sci. Total Environ.* 750, 141545. doi:10.1016/j.scitotenv.2020.141545

Zhang, Z., Li, M., Chen, W., Zhu, S., Liu, N., and Zhu, L. (2010). Immobilization of lead and cadmium from aqueous solution and contaminated sediment using nano-hydroxyapatite. *Environ. Pollut.* 158, 514–519. doi:10.1016/j.envpol.2009.08.024

Zhang, Z., Wang, T., Zhang, H., Liu, Y., and Xing, B. (2021). Adsorption of Pb(II) and Cd(II) by magnetic activated carbon and its mechanism. *Sci. Total Environ.* 757, 143910. doi:10.1016/j.scitotenv.2020.143910

Zhao, J., Liu, J., Li, N., Wang, W., Nan, J., Zhao, Z., et al. (2016). Highly efficient removal of bivalent heavy metals from aqueous systems by magnetic porous Fe$_3$O$_4$-MnO$_2$: Adsorption behavior and process study. *Chem. Eng. J.* 304, 737–746. doi:10.1016/j.cej.2016.07.003